nature chemical biology

ARTICLE

PUBLISHED ONLINE: 26 AUGUST 2012 | DOI: 10.1038/NCHEMBIO.1060

Pyruvate kinase M2 activators promote tetramer formation and suppress tumorigenesis

Dimitrios Anastasiou[1,2,13], Yimin Yu[3,13], William J Israelsen[3,13], Jian-Kang Jiang[4], Matthew B Boxer[4], Bum Soo Hong[5], Wolfram Tempel[5], Svetoslav Dimov[5], Min Shen[4], Abhishek Jha[6], Hua Yang[7], Katherine R Mattaini[3], Christian M Metallo[8], Brian P Fiske[3], Kevin D Courtney[1,2,9], Scott Malstrom[3], Tahsin M Khan[3], Charles Kung[7], Amanda P Skoumbourdis[4], Henrike Veith[4], Noel Southall[4], Martin J Walsh[4], Kyle R Brimacombe[4], William Leister[4], Sophia Y Lunt[3], Zachary R Johnson[3], Katharine E Yen[7], Kaiko Kunii[7], Shawn M Davidson[3], Heather R Christofk[1], Christopher P Austin[4], James Inglese[4], Marian H Harris[10], John M Asara[1,11], Gregory Stephanopoulos[6], Francesco G Salituro[7], Shengfang Jin[7], Lenny Dang[7], Douglas S Auld[4], Hee-Won Park[5,12], Lewis C Cantley[1,2], Craig J Thomas[4] & Matthew G Vander Heiden[3,9]*

Cancer cells engage in a metabolic program to enhance biosynthesis and support cell proliferation. The regulatory properties of pyruvate kinase M2 (PKM2) influence altered glucose metabolism in cancer. The interaction of PKM2 with phosphotyrosine-containing proteins inhibits enzyme activity and increases the availability of glycolytic metabolites to support cell proliferation. This suggests that high pyruvate kinase activity may suppress tumor growth. We show that expression of PKM1, the pyruvate kinase isoform with high constitutive activity, or exposure to published small-molecule PKM2 activators inhibits the growth of xenograft tumors. Structural studies reveal that small-molecule activators bind PKM2 at the subunit interaction interface, a site that is distinct from that of the endogenous activator fructose-1,6-bisphosphate (FBP). However, unlike FBP, binding of activators to PKM2 promotes a constitutively active enzyme state that is resistant to inhibition by tyrosine-phosphorylated proteins. These data support the notion that small-molecule activation of PKM2 can interfere with anabolic metabolism.

Cancer cells differ from many normal cells in the way they use extracellular nutrients, providing a strategy to interfere with tumor growth[1,2]. The increased cell proliferation that characterizes tumor growth creates an enhanced need for biological building blocks to support the production of new cells[3]. To meet this increased biosynthetic demand, cancer cells have higher uptake of nutrients such as glucose. In addition, the metabolic pathways of cancer cells are altered to allow production of macromolecules and withstand the oxidative stress that is associated with tumorigenesis[1,3–6].

Enhanced glucose uptake is a hallmark of several cancers and is used in the clinic as a diagnostic tool through positron emission tomography imaging of the glucose analog ^{18}F-deoxyglucose[7]. Moreover, in contrast to most normal tissues, where much of the glucose is oxidized through the tricarboxylic acid cycle in the mitochondria, cancer cells preferentially convert glucose to lactate[3]. The fate of glucose inside cells is influenced by the enzymatic properties of the specific glycolytic gene products that are expressed. Expression of PKM2 can contribute to the characteristic glucose metabolism of tumors, and replacement of PKM2 with its splice variant PKM1 cannot efficiently support biosynthesis and tumor growth[8]. Thus, pyruvate kinase regulates a step in glucose metabolism that can be crucial for controlling cell proliferation.

Pyruvate kinase catalyzes the last step of glycolysis, transferring the phosphate from phosphoenolpyruvate (PEP) to ADP to yield ATP and pyruvate. In mammals, two genes encode a total of four pyruvate kinase isoforms. The *Pkrl* gene encodes the PKL and PKR isoforms of pyruvate kinase, which are expressed in the liver and red blood cells, respectively. Most tissues express either the PKM1 or PKM2 isoform encoded by the *Pkm* gene. PKM1 is found in many normal differentiated tissues, whereas PKM2 is expressed in most proliferating cells, including in all cancer cell lines and tumors tested thus far[9]. PKM1 and PKM2 are derived from alternative splicing of a *Pkm* gene transcript by mutual exclusion of a single conserved exon encoding 56 amino acids[10–12]. Despite their very similar primary sequences, PKM1 and PKM2 have different catalytic and regulatory properties. PKM1 has high constitutive enzymatic activity[13]. In contrast, PKM2 is less active but can be allosterically activated by the upstream glycolytic metabolite FBP[14]. It has been hypothesized that FBP binding induces conformational

[1]Department of Medicine, Division of Signal Transduction, Beth Israel Deaconess Medical Center, Boston, Massachusetts, USA. [2]Department of Systems Biology, Harvard Medical School, Boston, Massachusetts, USA. [3]Koch Institute for Integrative Cancer Research, Massachusetts Institute of Technology Cambridge, Massachusetts, USA. [4]National Institutes of Health (NIH) Chemical Genomics Center, National Center for Advancing Translational Sciences, NIH, Bethesda, Maryland, USA. [5]Structural Genomics Consortium, University of Toronto, Toronto, Ontario, Canada. [6]Department of Chemical Engineering, Massachusetts Institute of Technology, Cambridge, Massachusetts, USA. [7]Agios Pharmaceuticals, Cambridge, Massachusetts, USA. [8]Department of Bioengineering, University of California, San Diego, California, USA. [9]Dana-Farber Cancer Institute, Harvard Medical School, Boston, Massachusetts, USA. [10]Department of Pathology, Children's Hospital, Boston, Massachusetts, USA. [11]Department of Medicine, Harvard Medical School, Boston, Massachusetts, USA. [12]Department of Pharmacology, University of Toronto, Toronto, Ontario, Canada. [13]These authors contributed equally to this work. *e-mail: mvh@mit.edu

changes that promote the association of the protein into homotetramers that comprise the most active form of the enzyme[15,16].

Unlike other pyruvate kinase isoforms, PKM2 can interact with proteins harboring phosphorylated tyrosine residues, leading to the release of FBP, which, in turn, reduces the activity of the enzyme[17]. Low PKM2 activity, in conjunction with increased glucose uptake, facilitates the flux of glucose carbons into the anabolic pathways that are derived from glycolysis[3,9,17,18]. Also, PKM2, but not PKM1, can be inhibited by direct oxidation of Cys358 as an adaptive response to increased intracellular reactive oxygen species[19]. Additionally, PKM2 expression in cancer cells is associated with enhanced phosphorylation of His11 on phosphoglycerate mutase 1 (PGAM1) by PEP[20]. This pathway provides an alternative route for pyruvate production while bypassing the generation of ATP during the pyruvate kinase step and thereby allows glycolysis to proceed at high rates[21]. Replacement of PKM2 with the constitutively active isoform PKM1 results in reduced lactate production, enhanced oxygen consumption and a decrease in PGAM1 phosphorylation[8,20]. Furthermore, there seems to be selection for PKM2 expression for growth *in vivo*. However, it is also possible that PKM2 expression reflects selection against high pyruvate kinase activity and therefore against expression of PKM1, raising the possibility that activation of PKM2 may impede cancer-cell proliferation by interfering with regulatory mechanisms that are crucial for proliferative metabolism.

Recently, we identified small molecules that selectively activate PKM2 over other pyruvate kinase isoforms *in vitro*[22,23]. Here we show that synthetic PKM2 activators can increase PKM2 activity in cells to levels that are comparable to the expression of PKM1. PKM2 activators bind to a pocket at the PKM2 subunit interface and thereby enhance association of PKM2 subunits into stable tetramers. Notably, this mechanism of tetramer stabilization is refractory to inhibition by tyrosine-phosphorylated proteins and influences cell metabolism. Among the two classes of PKM2 activators described here, a member of the thieno[3,2-b]pyrrole[3,2-d]pyridazinones class, TEPP-46, has pharmacokinetic properties that are amenable to experiments in mice. Expression of PKM1 in tumors in mice or continuous dosing of mice with TEPP-46 decreases the development of human cancer cell xenografts, suggesting that increased pyruvate kinase activity can impair tumorigenesis.

RESULTS

Increased pyruvate kinase activity impairs tumor growth

We have previously shown that replacement of PKM2 with PKM1 impairs the ability of H1299 human non–small-cell lung cancer cells to form xenograft tumors in mice[8]. This observation may reflect selection for PKM2 expression in tumors. However, because the ability to decrease PKM2 activity correlates with increased cell proliferation[17], it is also possible that the high pyruvate kinase activity that is associated with the expression of the constitutively active PKM1 isoform can suppress tumor growth. To address whether PKM1 expression alone affects tumor formation *in vivo*, we engineered H1299 cells to stably express Flag-tagged PKM1 (Flag-PKM1) in the presence of endogenous PKM2 (henceforth referred to as H1299-PKM1 cells). Expression of Flag-PKM1 did not affect the endogenous PKM2 levels in these cells (**Supplementary Results**, **Supplementary Fig. 1a**) but did result in a 35% ± 17% s.d. increase in total cellular pyruvate kinase activity (**Fig. 1a**). Both PKM1 and PKM2 can associate into tetramers[24,25]. To determine whether PKM1 can associate with endogenous PKM2, we used an antibody to Flag to immunoprecipitate Flag-PKM1. SDS-PAGE of the immunoprecipitated protein followed by silver staining revealed the presence of stoichiometric amounts of Flag-PKM1 and endogenous coprecipitating PKM2 (**Supplementary Fig. 1b**). The identity of PKM2 was confirmed by MS (**Supplementary Fig. 1c**). These data show that PKM1 can form heterocomplexes with endogenous PKM2 and that immunoprecipitation of exogenously expressed Flag-tagged pyruvate kinase can be used to assess the formation of multimeric pyruvate kinase complexes in cells. Furthermore, these data suggest that expression of PKM1 in PKM2-expressing cells is sufficient to increase their total pyruvate kinase activity.

To determine whether PKM1 expression with enhanced pyruvate kinase activity interferes with tumor growth, we compared the ability of H1299-PKM1 cells and parental H1299 cells to form tumors in immunocompromised (*nu/nu*) mice. Tumors emerged in every site where parental cells were injected after a median time of 31.5 d (**Fig. 1b**). However, only four out of ten sites injected with H1299-PKM1 cells gave rise to tumors. Notably, tumors derived from H1299-PKM1 cells were significantly (P = 0.0148) smaller (**Fig. 1c**), formed later and had reduced expression of Flag-PKM1 relative to the injected H1299-PKM1 cells (**Fig. 1d** and **Supplementary Fig. 2**). Furthermore, pyruvate kinase activity was consistently lower in tumor lysates than in parental H1299 cells (**Fig. 1e**). As the same numbers of parental and PKM1-expressing cells were injected to initiate tumors, the low pyruvate kinase activity in all the tumors suggests that the small tumors derived from the H1299-PKM1 cells arose from a subset of cells that lost PKM1 expression. These data support the notion that decreased pyruvate kinase activity is associated with

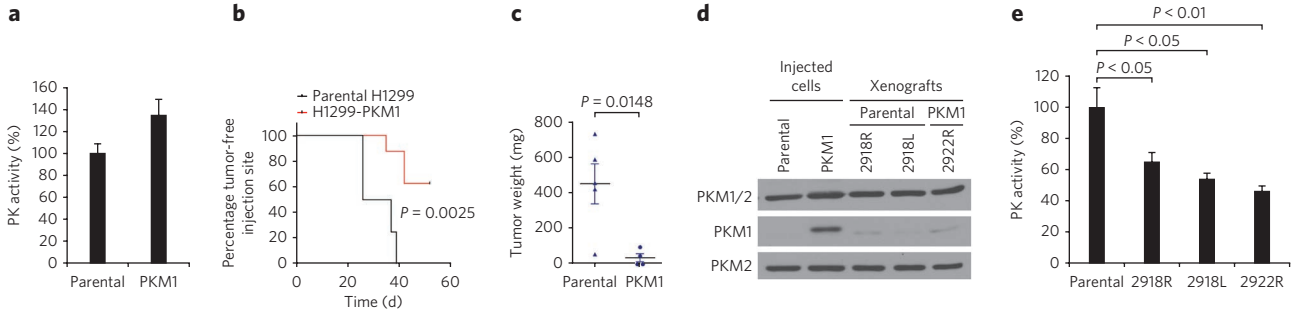

Figure 1 | PKM1 expression in cancer cells impairs xenograft tumor growth. (**a**) Pyruvate kinase (PK) activity in H1299 human lung cancer cells infected with a retrovirus to stably express Flag-PKM1 (referred to as H1299-PKM1 cells in the text) or empty vector (Parental) and then lysed. Data are shown as mean ± s.d. (**b**) Tumor formation over time of parental or H1299-PKM1 cells generated as in **a** and injected subcutaneously at equal numbers in *nu/nu* mice. The *P* value shown was calculated by log-rank (Mantel-Cox) test. (**c**) Final tumor weights from the experiment in **b**. Mean tumor weights ± s.e.m. are shown, and the *P* value was calculated by unpaired Student's *t* test. (**d**) Expression of Flag-PKM1 and endogenous PKM2 in the cells used in **b** and **c** determined by western blotting with an antibody that recognizes both PKM1 and PKM2 (PKM1/2) or with isoform-specific antibodies. The uncropped blots are shown in **Supplementary Figure 10**. (**e**) Pyruvate kinase activity assays in lysates of the tumors shown in **d**. The *P* values shown were calculated by one-way analysis of variance and Tukey's post test. In **d** and **e**, 2918R, 2918L and 2922R refer to the animal number and the site injected (L, left; R, right). The average value derived from three lysates is shown as mean ± s.e.m.

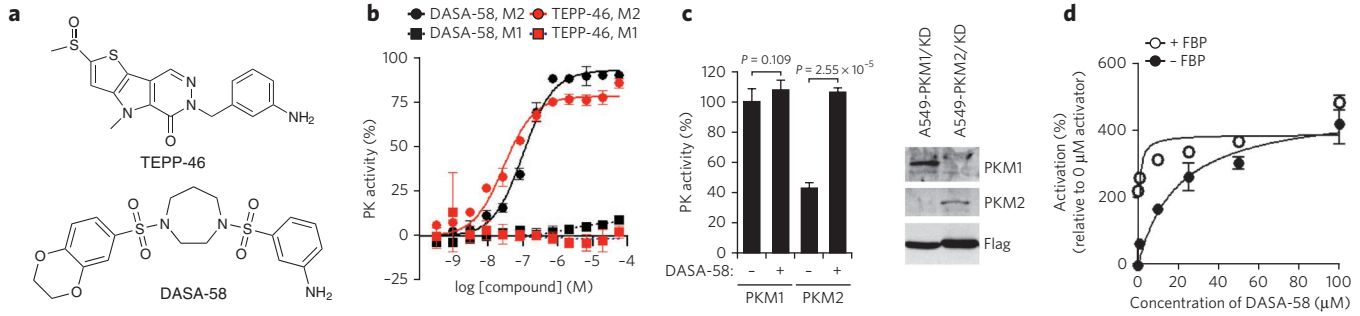

Figure 2 | TEPP-46 and DASA-58 isoform specificity *in vitro* and in cells. (**a**) Structures of the PKM2 activators TEPP-46 and DASA-58. (**b**) Pyruvate kinase (PK) activity in purified recombinant human PKM1 or PKM2 expressed in bacteria in the presence of increasing concentrations of TEPP-46 or DASA-58. M1, PKM1; M2, PKM2. Data represent mean ± s.d. (**c**) Pyruvate kinase activity in lysates of A549 cells engineered to stably express Flag-PKM1 or Flag-PKM2 in the absence of endogenous PKM2, which was knocked down with short hairpin RNA[8]. Cells were treated with DMSO or 40 μM DASA-58 for 3 h prior to lysis[8]. Also shown is a western blot using isoform-specific antibodies confirming expression of Flag-PKM1 and Flag-PKM2 in the cells (right). Data shown are mean ± s.d. from three lysates. The *P* values shown were calculated by Student's *t* test. Similar results were observed in H1299 cells (data not shown). The uncropped blots are shown in **Supplementary Figure 10**. (**d**) Pyruvate kinase activity in the presence or absence of 200 μM FBP in A549 cells treated with the indicated doses of DASA-58 for 3 h and then lysed. Data represent mean ± s.d.

tumor growth and suggest that high pyruvate kinase activity can suppress the formation of cancer cell xenograft tumors in mice.

Small molecules can specifically activate PKM2 in cells

A recent screen identified two structurally distinct classes of small-molecule PKM2 activators[22,23]. A representative compound from each class was selected for further studies: the thieno-[3,2-b]pyrrole[3,2-*d*]pyridazinone NCGC00186528 (TEPP-46; ML265, PubChem CID 44246499) and the substituted *N*,*N*′-diarylsulfonamide NCGC00185916 (DASA-58; ML203, PubChem CID 44543605) are both potent activators of recombinant PKM2 (TEPP-46: 90% maximum activating concentration (AC_{90}) = 470 nM, half-maximum activating concentration (AC_{50}) = 92 nM; DASA-58: AC_{90} = 680 nM, AC_{50} = 38 nM; **Fig. 2a**) and are soluble in aqueous solution[22,23]. Furthermore, TEPP-46 and DASA-58 are selective for PKM2, as they do not activate recombinant PKM1 *in vitro* (**Fig. 2b**). To investigate whether these compounds are able to activate PKM2 selectively in cells, we engineered A549 cells to express Flag-PKM1 or Flag-PKM2 with concomitant knockdown of endogenous PKM2 (referred to as A549-PKM1/KD or A549-PKM2/KD cells, respectively) (**Fig. 2c**). We treated these cells with 40 μM DASA-58 and assayed pyruvate kinase activity in the corresponding cell lysates. Consistent with our results in the H1299 cells, lysates from DMSO-treated A549-PKM1/KD cells had 233% ± 27% s.d. more pyruvate kinase activity than A549-PKM2/KD cells. We found no increase in pyruvate kinase activity after treatment of A549-PKM1/KD cells with DASA-58; however, DASA-58 treatment resulted in a 248% ± 21% s.d. increase of pyruvate kinase activity in A549-PKM2/KD cell lysates. These data suggest that DASA-58 can selectively activate PKM2 in cells.

In a manner analogous to that of FBP, both TEPP-46 and DASA-58 decrease the K_m of PKM2 for PEP with no effect on its K_m for ADP[22,23], suggesting that TEPP-46 and DASA-58 activate PKM2 by a mechanism similar to that of the endogenous activator FBP. To determine whether FBP could further activate PKM2 in activator-treated cells, we incubated A549 cells with increasing concentrations (0–100 μM) of DASA-58 and assayed PKM2 activity in the corresponding lysates in the presence or absence of FBP. In the absence of FBP, DASA-58 activated PKM2 in a dose-dependent manner, with an effective cellular half-activation concentration (EC_{50}) of 19.6 μM (**Fig. 2d**). However, in the presence of high physiological concentrations of FBP (200 μM), we found no additional increase in activity as a result of treatment with the activator DASA-58. These data are consistent with the *in vitro* kinetic analysis suggesting that DASA-58 enhances PKM2 activity by a mechanism similar to that of FBP.

PKM2 activators stabilize subunit interactions

The most active form of PKM2 is a tetramer, and subunit association is thought to be promoted by FBP. To test this hypothesis, we separated bacterially expressed recombinant PKM2 into monomers and tetramers by size-exclusion chromatography (**Supplementary Fig. 3a**) and assayed the ability of FBP to increase PKM2 activity. PKM2 tetramers showed greater than 50-fold higher activity than PKM2 monomers (**Supplementary Fig. 3b**). The addition of FBP had minimal effects on PKM2 tetramer activity (consistent with bacterial FBP being trapped on the stable tetramers[17]), but FBP increased the activity of PKM2 monomers by approximately 70% (**Supplementary Fig. 3c**). The relatively modest activation of the monomers probably reflects the slow kinetics of assembling tetramers from monomers under dilute conditions. To determine whether activation of monomers by FBP is accompanied by changes in PKM2 subunit composition, we performed sucrose gradient ultracentrifugation on purified recombinant PKM2. Under these conditions, the majority of the PKM2 was found to dissociate into monomers (**Fig. 3a**). Exposure of PKM2 to FBP throughout the experiment resulted in a shift of the protein into a tetrameric configuration that was comparable to that of the constitutively active PKM1 isoform (**Supplementary Fig. 3d**). To investigate whether small-molecule activators also promote the association of pyruvate kinase subunits into tetramers, we incubated purified PKM2 with TEPP-46 or DASA-58. We found only a partial shift of PKM2 into tetramers with either activator alone (**Supplementary Fig. 3d**). As only a fraction of bacterially expressed PKM2 is bound to FBP (**Supplementary Fig. 3a–c**), we reasoned that the activators might only stabilize FBP-bound PKM2. Consistent with this hypothesis, transient incubation of PKM2 with FBP before the addition of TEPP-46 resulted in the activator fully stabilizing the PKM2 tetramer. Overall, these data suggest that, unlike PKM2, PKM1 is a stable tetrameric enzyme and both FBP and small-molecule activators increase PKM2 activity by promoting the tetrameric state.

To investigate whether PKM2 activators promote pyruvate kinase subunit association in cells, we generated A549 cells stably expressing Flag-PKM1 or Flag-PKM2 and treated them with DMSO or DASA-58. After lysis and immunoprecipitation with Flag antibodies, we determined the relative amount of endogenous PKM2 that coprecipitated under the various conditions by western blot using an antibody that recognizes an epitope that is common

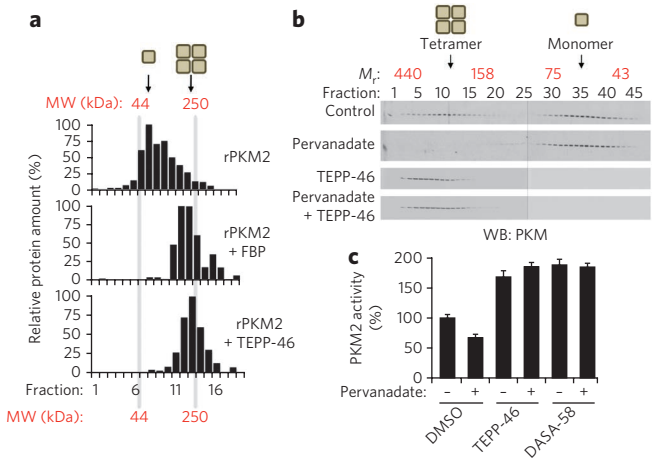

Figure 3 | Activators promote PKM2 tetramer formation and prevent inhibition by phosphotyrosine signaling. (**a**) Sucrose gradient ultracentrifugation profiles of purified recombinant PKM2 (rPKM2) and the effects of FBP and TEPP-46 on PKM2 subunit stoichiometry. Recombinant PKM2 was transiently exposed to FBP before addition of TEPP-46. After centrifugation, fractions were collected and analyzed for relative amounts of PKM2. MW, molecular weight. (**b**) The stoichiometry of PKM2 subunit association as determined by western blot (WB) using a pyruvate kinase antibody of the chromatographic fractions of A549 cells treated with 100 μM pervanadate for 10 min in the presence or absence of TEPP-46, lysed hypotonically and analyzed by size-exclusion chromatography. M_r, relative molecular weight. Uncropped blots are shown in **Supplementary Figure 10**. (**c**) Pyruvate kinase activity in A549 cells treated with pervanadate as in **b** in the presence of DMSO, 1 μM TEPP-46 or 1 μM DASA-58. $P < 0.0001$ for comparison between DMSO and each of the other conditions, calculated by two-way analysis of variance. Data represents mean ± s.e.m.

to both pyruvate kinase isoforms. Flag-PKM1 immunoprecipitated equivalent amounts of endogenous PKM2 irrespective of activator treatment (**Supplementary Fig. 3e**). In contrast, DASA-58 treatment resulted in increased amounts of endogenous PKM2 immunoprecipitating with Flag-PKM2 when compared with DMSO-treated cells or cells treated with an inactive analog of DASA-58 (ref. 23). Similar results were obtained with TEPP-46 (**Supplementary Fig. 3f**). These data indicate that PKM2 activators can promote the stable association of PKM2 subunits in cells.

The interaction of phosphotyrosine with PKM2 downstream of growth factor signaling is crucial for both cell proliferation and metabolic changes that promote anabolism[17]. Binding to phosphotyrosine decreases PKM2 activity by catalyzing the release of FBP from the enzyme[17,26]. Pervanadate inhibits tyrosine phosphatases to acutely increase the amounts of tyrosine-phosphorylated proteins, and treatment of cells with pervanadate results in inhibition of PKM2, but not PKM1, activity[17,20]. To determine whether the inhibition of PKM2 activity caused by increased tyrosine phosphorylated proteins results in destabilization of PKM2 tetramers in cells, we treated cells with pervanadate and determined the stoichiometry of the PKM2 subunit composition by size-exclusion chromatography. In logarithmically growing A549 cells, approximately half of the PKM2 eluted as a tetramer, whereas half dissociated into monomers during size-exclusion chromatography (**Fig. 3b**). Under these conditions, we did not detect a substantial population of dimeric PKM2. Pervanadate treatment caused the disappearance of PKM2 tetramers, and the entire PKM2 population was detected as monomers in this assay. We then tested whether PKM2 activators influence the regulation of PKM2 tetramerization by tyrosine-phosphorylated proteins. In logarithmically growing cells treated with TEPP-46, all of the PKM2 was found as a tetramer (**Fig. 3b**). Moreover, PKM2 tetramers were preserved even after treating the cells with pervanadate (**Fig. 3b**). Similar results were obtained with H1299 cells (**Supplementary Fig. 3g**).

To test whether PKM2 activators also affect PKM2 activity when the amounts of tyrosine-phosphorylated proteins are increased, we assayed PKM2 activity in lysates of cells treated with DMSO, TEPP-46 or DASA-58 and then with pervanadate. Pretreatment of cells with TEPP-46 or DASA-58 prevented pervanadate-induced inhibition of PKM2 activity (**Fig. 3c**). It is plausible that activator binding renders PKM2 resistant to an inhibitory modification induced by pervanadate treatment. However, a phosphotyrosine-containing peptide corresponding to the optimal PKM2 interaction motif[17] can promote the dissociation of PKM2 tetramers (**Supplementary Fig. 3h**) but does not inhibit the ability of TEPP-46 to activate recombinant PKM2 (**Supplementary Fig. 3i**). These results indicate that activators render PKM2 tetramers resistant to the dissociation induced by phosphotyrosine signaling.

Overall, these data argue that PKM2 activators enhance PKM2 activity by promoting the stable (active) tetrameric form of PKM2. However, similar to PKM1 but unlike the endogenous activator FBP, small-molecule PKM2 activators promote the active form of the enzyme even in the presence of increased amounts of phosphotyrosine that would otherwise lower PKM2 activity.

Structural analysis of the mode of binding of PKM2 activators

On the basis of these biochemical studies, it is possible that these agents activate PKM2 by binding at the same site as FBP but are not released after interaction with phosphotyrosine. Alternatively, PKM2 activators may stabilize the tetramer in another way. To explore these possibilities, purified recombinant PKM2 was crystallized in the presence of TEPP-46 or DASA-58. Our refined model shows that one tetrameric PKM2 contains two activators and four FBP molecules (**Fig. 4a**, **Supplementary Table 1** and **Supplementary Fig. 4a**). The four FBP molecules were copurified from the *Escherichia coli* cells where the PKM2 was produced, and they were found to occupy all four of the FBP binding pockets of the PKM2 tetramer. In comparison, one activator was found in the interface (named A-A′) between the A domains of each dimer approximately 35 Å away from the FBP binding pocket (**Fig. 4a** and **Supplementary Fig. 4a**). The bound activator was completely buried within the A-A′ interface. The activator binding pocket was lined with equivalent sets of residues provided by each of the PKM2 molecules forming the A-A′ interface, where the activator was accommodated through polar and van der Waals interactions with pocket-lining residues (**Fig. 4b** and **Supplementary Fig. 4b**). Particularly for TEPP-46, the crystallographic evidence suggested that the binding orientation of the activator alternates based on a pseudo–two-fold axis that is co-linear with both the nitrogen-methyl carbon bond of the N-methyl pyrrole moiety of TEPP-46 and the pseudo–two-fold axis of the A-A′ interface. The extra space in the pocket was filled with solvent molecules or ions, which also mediate hydrogen bonds between the activator and the pocket-lining residues (**Fig. 4b**). These data show that TEPP-46 and DASA-58 bind PKM2 through a binding pocket that is distinct from that of FBP and that they stabilize a tetrameric conformational state.

FBP is thought to contribute to tetramer formation by stabilizing the C-C′ interface. Given the distinct location of the activator binding pocket, we investigated whether activator binding results in the stabilization of subunit interaction along the A-A′ interface. A recent study showed that acetylation of Lys305 results in decreased PKM2 subunit association, an alternative way to inactivate the enzyme[27]. The ε-amino group of Lys305 interacts through a salt bridge with Glu384 in the neighboring subunit along the A-A′ interface (**Supplementary Fig. 4c**). Acetylation may interfere with this interaction, resulting in destabilization of the PKM2 tetramer.

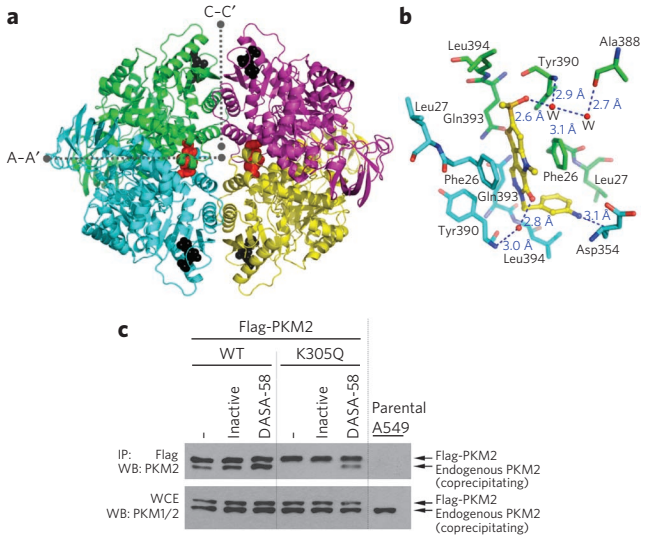

Figure 4 | Structural analysis of the PKM2 activator mode of action. (**a**) Interaction between tetrameric PKM2 and TEPP-46. The four PKM2 monomers are represented in cartoon mode with different colors. The bound FBP and the activator molecules are colored black and red, respectively, and are shown as space-filling models. The interfaces between two monomers are indicated by dotted lines. (**b**) The interactions between TEPP-46 and the surrounding residues. The bound activator is colored yellow and represented by a ball and stick model. The residues from the two monomers that are involved in the interaction are labeled and colored green and cyan. Hydrogen bonds are indicated by blue dashed lines with their distances indicated. (**c**) DASA-58 stabilizes the interaction of Flag-PKM2^{K305Q} with endogenous PKM2. Coprecipitating endogenous PKM2 in lysates from A549 cells stably expressing Flag-PKM2 (WT) or Flag-PKM2^{K305Q} as assessed by western blotting using an antibody that recognizes PKM2 or both PKM1 and PKM2 (PKM1/2). IP, immunoprecipitation; WCE, whole cell extracts. Uncropped blots are shown in **Supplementary Figure 10**.

We therefore mutated Lys305 to glutamine to mimic acetylation. Flag-PKM2 with the K305Q mutation did not coprecipitate endogenous PKM2 (**Fig. 4c**). Given that the activator binds between two PKM2 subunits at the A-A′ interface where Lys305 and Glu384 reside, we investigated whether the PKM2 activator DASA-58 can rescue the interaction between Flag-PKM2^{K305Q} and endogenous PKM2. Indeed, treatment of cells with DASA-58 restored the ability of Flag-PKM2^{K305Q} to coprecipitate endogenous PKM2 (**Fig. 4c**). These data further support a model in which PKM2 activators function by binding at the A-A′ interface and stabilize the PKM2 tetramer and suggest that the activators could circumvent *in vivo* mechanisms for the inhibition of PKM2 activity.

PKM2 activators alter metabolism in cultured cells

Overall, our results suggest that PKM2 activators mimic the regulatory properties of constitutively active PKM1, thereby promoting high PKM2 activity regardless of the mechanisms cells use to decrease pyruvate kinase activity. Therefore, we next examined the effects of activator treatment on cellular proliferation. Similar to results obtained when PKM2 is replaced with PKM1 (ref. 8), under standard tissue culture conditions, PKM2 activators had no effect on cell proliferation when tested across several lines (**Fig. 5a** and **Supplementary Fig. 5**). In contrast, when we assayed cellular proliferation under hypoxic conditions (1% O_2), PKM2 activator treatment resulted in a decreased rate of cell proliferation compared to DMSO treatment (**Fig. 5a**). Similarly, expression of PKM1 in the presence of endogenous PKM2 had no effect on cell proliferation in standard tissue culture conditions but inhibited cell proliferation under hypoxia to a similar degree as treatment with activators. These observations are consistent with previous data showing that replacement of PKM2 with PKM1 impairs cell proliferation under low oxygen conditions[8].

To test our hypothesis that PKM2 activators mimic the metabolic state found in PKM1-expressing cells, we interrogated the effects of activator treatment on cell metabolism. Replacement of PKM2 with PKM1 in cultured cells results in reduced lactate production and enhanced oxygen consumption[8]. Acute treatment of H1299 cells with DASA-58 also resulted in decreased lactate production (**Fig. 5b**). Unlike cells in which PKM2 is replaced with PKM1, expression of PKM1 in the presence of endogenous PKM2 or activator treatment had no effect on oxygen consumption (**Supplementary Fig. 6a**). Furthermore, DASA-58 treatment did not affect glucose or glutamine consumption (**Supplementary Fig. 6b**,**c**), indicating that changes in the uptake of major nutrients probably do not underlie the observed metabolic phenotypes. Inhibition of PKM2 activity mediated by phosphotyrosine signaling results in more efficient incorporation of glucose carbons into lipids[17]. To determine whether PKM2 activator treatment inhibits glucose carbon incorporation into lipids, cells were incubated with [6-^{14}C]glucose in the presence of DMSO or DASA-58, cellular lipids were extracted, and ^{14}C-labeled lipids were quantified by scintillation counting. DASA-58 treatment resulted in a significant (P = 0.009) decrease in the incorporation of

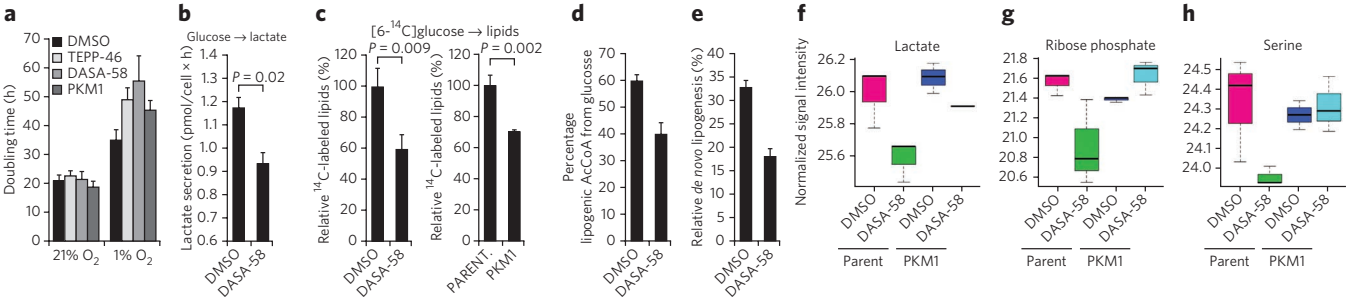

Figure 5 | Metabolic effects of cell treatment with PKM2 activators. (**a**) Effects of TEPP-46, DASA-58 (both used at 30 μM) or PKM1 expression on the doubling time of H1299 cells under normoxia (21% O_2) or hypoxia (1% O_2). (**b**) Effects of DASA-58 on lactate production from glucose. The P value shown was calculated by Student's t test. Data are mean ± s.d. from three biological replicates. (**c**) Lipid-incorporated ^{14}C by scintillation counting in cellular lipids extracted from logarithmically growing H1299 cells (left) or parental H1299 and H1299-PKM1 cells (right) incubated for 2 h with 4 μCi/ml [6-^{14}C]glucose in the presence of DMSO or 30 μM DASA-58. Data are mean ± s.d. P value was calculated using unpaired Student's t test. (**d**,**e**) Contribution of [U-$^{13}C_6$]glucose to the lipogenic AcCoA pool (**d**) and fractional new synthesis of palmitate (**e**) determined by isotopomer spectral analysis in A549 cells treated with DMSO or 100 μM DASA-58. Error bars indicate 95% confidence intervals. (**f**–**h**) Intracellular concentrations of lactate, ribose phosphate and serine in parental H1299 or H1299-PKM1 cells treated with DMSO or 25 μM of TEPP-46 for 36 h determined by targeted LC/MS/MS.

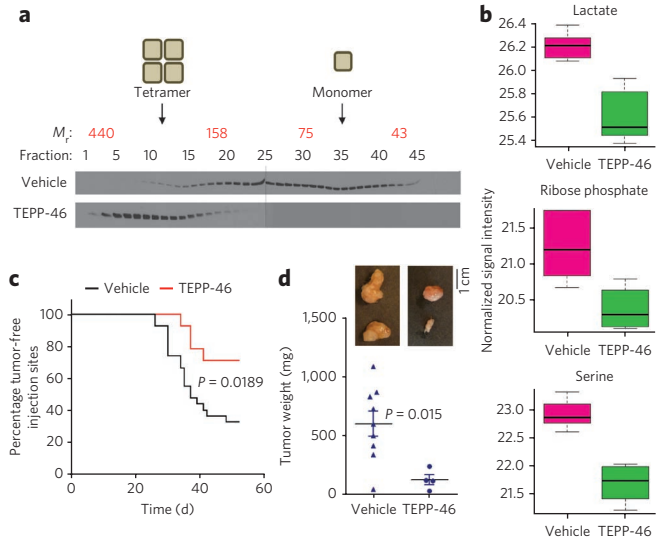

Figure 6 | PKM2 activators impair xenograft growth. (**a**) PKM2 complex stoichiometry in tumor lysates from mice bearing H1299 xenograft tumors that received bolus doses of TEPP-46 at 50 mg per kg body weight 16 h and 4 h before being euthanized as determined by size-exclusion chromatography. The uncropped blots are shown in **Supplementary Figure 10**. (**b**) Concentrations of lactate, ribose phosphate and serine in H1299 xenograft tumors from mice treated with vehicle or TEPP-46 as described in a. (**c**) Tumor emergence in *nu/nu* mice subcutaneously injected with H1299 cells and then given either vehicle or TEPP-46 at 50 mg per kg body weight twice daily throughout the duration of the experiment. The *P* value shown was calculated by log-rank (Mantel-Cox) test. (**d**) Final tumor weights after dissection at day 52. Mean tumor weights ± s.e.m. are shown, and the *P* value was calculated by unpaired Student's *t* test.

glucose-derived carbon into lipids (**Fig. 5c**). Similarly, we found a decrease in the incorporation of glucose-derived carbon into lipids in H1299-PKM1 cells (**Fig. 5c**). We also used gas chromatography MS (GC/MS) to analyze the metabolite extracts of cells incubated with ^{13}C-labeled glucose. DASA-58 treatment resulted in diminished incorporation of the glucose-derived carbons into acetyl–coenzyme A (AcCoA), which is used for *de novo* palmitate synthesis (**Fig. 5d** and **Supplementary Fig. 6d**), and a decrease in overall *de novo* lipogenesis (**Fig. 5e**). TEPP-46 also induced a decrease in the intracellular concentrations of AcCoA, lactate, ribose phosphate and serine (**Fig. 5f–h** and **Supplementary Fig. 6e**). Ribose phosphate is a key intermediate for the biosynthesis of nucleotides through the pentose phosphate pathway, and serine, in addition to being incorporated directly into proteins, can serve as a precursor for lipid head groups and glycine and also provide carbon to the folate pool. Notably, these changes, along with overall changes in other intracellular metabolite concentrations (**Supplementary Fig. 6f**), were evident only in parental cells and not PKM1-expressing cells, indicating that the effects of the activator on cellular metabolism are specific to PKM2. No differences in the concentrations of lactate, ribose phosphate and serine were found between PKM1-expressing and parental cells, probably reflecting that, unlike transient activation of PKM2 by small molecules, selection for PKM1 expression in cells may lead to adaptive changes in metabolite concentrations to compensate for the effects of chronic elevation of pyruvate kinase activity. Regardless, these data indicate that small-molecule activation of PKM2 can alter glucose metabolism and decrease the intracellular concentrations of intermediates that are required for biosynthesis.

Low PKM2 activity is also associated with increased phosphorylation of PGAM1 on the catalytic histidine residue (His11)[20]. To determine whether activator treatment decreases PGAM1 phosphorylation, we treated cells with DMSO or DASA-58 and analyzed the corresponding lysates by two-dimensional SDS-PAGE and isoelectric focusing to resolve the PGAM1 species in cells[20]. Similar to findings in PKM1-expressing cells[20], we found a decrease in PGAM1 phosphorylation as a result of activator treatment (**Supplementary Fig. 7**). Together, these data suggest that PKM2 activators induce a metabolic state in cells that is comparable to, but distinct from, that found with PKM1 expression.

A PKM2 activator inhibits xenograft tumor growth

PKM1 expression impairs the ability of cancer cells to grow *in vivo* as xenografts. To determine whether PKM2 activators also impede xenograft tumor growth, we determined the compound that would be suitable for experiments in mice. On the basis of *in vitro* absorption, distribution, metabolism and excretion (ADME) profiling studies, we predicted that TEPP-46 would have superior *in vivo* drug exposure compared to other analogs. To determine the appropriate repeated drug doses for the mouse experiments, we performed single-dose pharmacokinetic and acute pharmacodynamic studies with TEPP-46. **Supplementary Figure 8** shows the drug concentration in mouse plasma over time after a single intravenous, intraperitoneal or oral dose. TEPP-46 has good oral bioavailability with relatively low clearance, a long half-life and a good volume of distribution, parameters that predict for drug exposure in tumor tissues (**Supplementary Table 2**). An acute oral dose of TEPP-46 (150 mg per kg body weight) readily achieved the maximal PKM2 activation measured in A549 xenograft tumors (**Supplementary Fig. 9a**). To ensure that drug treatment could be carried out safely for a multiday dosing regimen, we also performed a 5-d repeat-dose tolerability study in mice and showed that a dose of 50 mg per kg body weight twice daily was well tolerated with no sign of weight loss (**Supplementary Fig. 9b**).

Because a twice-daily oral dose of 50 mg per kg body weight of TEPP-46 was well tolerated and led to reasonable drug plasma concentrations in mice, we tested whether this dose of TEPP-46 could promote PKM2 tetramerization in xenograft tumors. We treated mice bearing H1299 xenograft tumors with vehicle or TEPP-46 and analyzed tumor lysates by size-exclusion chromatography. In xenografts from vehicle-treated mice, very little of the PKM2 was found as tetramers (**Fig. 6a**). In contrast, tumors exposed to TEPP-46 harbored exclusively tetrameric PKM2. A metabolomic analysis revealed that, similar to the effects in cultured cells after treatment with TEPP-46, tumors derived from mice treated with TEPP-46 had lower concentrations of lactate, ribose phosphate and serine (**Fig. 6b**). We then tested whether these changes in PKM2 activity and tumor metabolism affect the ability of H1299 cells to form xenografts. H1299 cells were injected into immunocompromised (*nu/nu*) mice, and the mice were then randomly divided into two cohorts, one treated with vehicle and the other treated with 50 mg per kg body weight of TEPP-46, dosed twice daily for the duration of the experiment. No apparent toxicity was observed in any mice, despite having over 7 weeks of continuous drug exposure, based on blood counts and serum chemistries (**Supplementary Table 3**) as well as histological examination of blood, bone marrow, liver, kidney, heart and the gastrointestinal tract. Tumors in activator-treated mice emerged with a delayed latency compared to tumors in vehicle-treated mice (**Fig. 6c**). In addition, the tumors from activator-treated mice were significantly ($P = 0.015$) smaller than those arising in mice treated with vehicle (**Fig. 6d**). TEPP-46 was detectable in the tumors from activator-treated mice, suggesting that cells in the tumor were exposed to the drug.

These data show that cancer cells in xenograft tumors are exposed to TEPP-46 after several weeks of oral dosing and that this can mimic PKM1 expression to impair the growth of H1299 cells as xenograft tumors.

DISCUSSION

Cancer cells harbor genetic changes that allow them to increase their nutrient uptake and alter their metabolism to support anabolic processes, and interfering with this metabolic program is a strategy for cancer therapy[1,2]. Altered glucose metabolism in cancer cells is mediated in part by expression of PKM2, which has unique regulatory properties. Unlike its splice variant PKM1, which is found in many normal tissues, PKM2 is allosterically activated by FBP and can interact with tyrosine-phosphorylated proteins to release FBP and decrease enzyme activity. Thus, growth factor signaling promotes decreased PKM2 activity and availability of glycolytic metabolites for anabolic pathways that branch from glycolysis. This suggests that activation of PKM2 might oppose the effects of growth signaling and interfere with anabolic glucose metabolism.

Consistent with this hypothesis, our data show that high pyruvate kinase activity caused by PKM1 expression or small-molecule PKM2 activation impedes the ability of cancer cells to form tumors in mice. PKM1 can associate with endogenous PKM2 and form heterocomplexes that are likely to be insensitive to FBP regulation and thus have higher activity. Recent publications have described nonenzymatic functions for PKM2 (refs. 28–30). Although these nonclassical PKM2 activities may also have a role in tumor formation, our data suggest that the ability to decrease enzyme activity is a key property of the enzyme that may drive PKM2 selection in tumors. Furthermore, these experiments provide evidence that elevated pyruvate kinase activity can be incompatible with efficient tumor growth.

Small-molecule PKM2 activators can mimic the enzymatic properties of PKM1 in PKM2-expressing cells and alter cell metabolism. Our studies focused on DASA-58 and TEPP-46, which are representative of two classes of PKM2-activating compounds[22,23]. These small molecules induce changes in the kinetic properties of PKM2 that are identical to those induced by the endogenous PKM2 activator FBP, suggesting that PKM2 could adopt a PKM1-like state in cells when FBP is high, in the absence of phosphotyrosine signaling or both. To our surprise, structural analyses of the activators bound to PKM2 tetramers revealed a binding pocket at the interface of the subunit interaction that is distinct from the site of FBP binding. Furthermore, unlike FBP, which stabilizes the C-C′ interface of the active tetramer, the small-molecule activators stabilize the A-A′ interface. FBP was also observed in the crystals containing the small-molecule activators, and activators stabilize PKM2 tetramers more effectively in the presence of FBP. This raises the possibility that FBP binding is required for small-molecule activation and that stabilization of the A-A′ interface inhibits FBP release. Nevertheless, these compounds enhance PKM2 enzymatic activity in a manner that renders PKM2 resistant to inhibition by phosphotyrosine binding, and interaction with phosphotyrosine is the only mechanism that has been described to release FBP from PKM2. No natural ligands have been identified that bind PKM2 in the same site as the PKM2 activators, but given that multiple activator classes bind in the same pocket, it is possible that this represents a previously unknown site of pyruvate kinase regulation.

Our findings are consistent with PKM2 existing in a monomer-tetramer equilibrium that can be altered by the presence of FBP, TEPP-46 or DASA-58. Although our results agree with previous reports showing that the fully associated tetrameric form of PKM2 is the active form of the enzyme, dimeric PKM2 was not a predominant form of the enzyme observed in our assays. Previous studies have described PKM2 dimers using isoelectric focusing chromatography[9]. It is possible that the methods we used to assess the PKM2 multimeric state favor complete tetramer dissociation to monomers. We suspect that much of the PKM2 *in vivo* exists in an equilibrium between loosely associated tetramers with low activity and tightly associated tetramers with high activity and that this equilibrium is influenced by FBP concentrations and phosphotyrosine signaling or post-translational modifications that destabilize the loosely associated (low activity) tetramer[17,19,26,27].

PKM2 activators may impair tumor-cell proliferation by interfering with anabolic metabolism. Activator treatment *in vitro* and *in vivo* results in decreased pools of ribose-phosphate and serine, which are key precursors for nucleotide, lipid and amino acid metabolism. However, no changes in the metabolite pools were found when pyruvate kinase activity was elevated by chronic PKM1 expression *in vitro*, suggesting that the metabolic states elicited by these two treatments might not be equivalent. It is possible that this response to PKM1 expression reflects adaptive events that can more effectively compensate for increased pyruvate kinase activity *in vitro*. PKM2 activator treatment also reduced the incorporation of glucose carbons into lactate and lipids, thus interfering with the increased lactate production used by many tumors to establish a redox balance that is compatible with high glycolytic rates[3]. Lipids are essential components of new cells, and reduced lipid production has been shown to inhibit cellular proliferation[31]. Notably, the effects of PKM2 activation on proliferation in cell culture are only evident under hypoxic conditions, suggesting that glucose-dependent anabolic pathways may only be crucial for proliferation under certain conditions. Oxidation-induced inhibition of PKM2 under hypoxia may support production of NADPH through the oxidative branch of the pentose phosphate pathway to sustain antioxidant responses[19]. Although the source of NADPH for biosynthetic processes, including lipid synthesis, remains a subject of active investigation, the ability of PKM2 to control cellular redox state may partially underlie the selective effects of PKM2 activation on proliferation under hypoxia.

Although our data indicate that small-molecule activation of PKM2 can impede the proliferation of cancer cells in xenograft models, it remains to be determined whether such compounds will be similarly effective in autochthonous mouse tumor models or will be efficacious as a cancer therapy in humans. PKM2 activators can also sensitize cells to oxidative-stress–induced death, raising the possibility that such compounds could enhance tumor killing in combination with drugs that increase cellular reactive oxygen species[6,19]. Regardless, this study further supports the notion that pyruvate kinase acts as a key regulatory node in glycolysis to control glucose fate in cells and argues that high pyruvate kinase activity is not conducive to the anabolic metabolism that is necessary for tumor growth.

METHODS

Mouse studies. All mouse studies were performed in accordance with institutional guidelines and approved by the Massachusetts Institute of Technology committee on animal care. Full experimental details are included in the **Supplementary Methods**.

Cell culture. 293T and A549 cells were cultured in standard DMEM-based media, and H1299, TT, SN12C and SKMel28 cells were cultured in RPMI-based media. For all hypoxia experiments, the media were supplemented with 20 mM HEPES. Cells expressing specific Flag-tagged isoforms of mouse pyruvate kinase M, or mutants thereof, in the absence of endogenous PKM2 were derived as previously described[8]. The cell doubling time was calculated by periodic measurement of cell mass accumulation over 6 d using crystal violet staining. Cell viability was assayed using CellTiter96 AQueous (Promega) or MTS (3-(4,5-dimethylthiazol-2-yl)-5-(3-carboxymethoxyphenyl)-2-(4-sulfophenyl)-2H-tetrazolium) assay (Promega) according to the manufacturer's instructions.

Western blotting. Cell or tissue lysates were analyzed by SDS-PAGE and western blotting using standard protocols and the following primary antibodies: anti-pyruvate kinase (Abcam, ab6191, dilution 1:2,000–1:5,000), anti-PKM1 (Sigma, SAB4200094, dilution 1:5,000), anti-PKM2 (Cell Signaling, 4053, dilution 1:1,000), anti-Flag (Sigma, F3165, dilution 1:5,000) and anti-actin (Abcam, ab1801, dilution 1:5,000). Where indicated, Flag-agarose (Sigma-A2220) was used for the immunoprecipitation of Flag-tagged proteins. Isoelectric focusing and two-dimensional SDS-PAGE western blot analyses were performed as described previously[20].

Xenograft experiments. H1299 cells with and without constitutive expression of mouse PKM1 were suspended in sterile PBS, and 5×10^6 cells were injected subcutaneously into *nu*/*nu* mice. Tumor growth was monitored, mice were euthanized after the time indicated, and tumors were harvested for analysis.

PKM2 activity. Pyruvate kinase activity was measured as described previously[32]. Where indicated, 100 μM pervanadate was added 10 min before cell lysis. For the phosphotyrosine peptide experiments, the amino acid sequences of the peptides were: GGAVDDDYAQFANGG (M2tide) and GGAVDDDpYAQFANGG (P-M2tide)[17].

Sucrose-gradient ultracentrifugation. Recombinant PKM2 was incubated with 500 nM TEPP-46, 1 μM DASA-58 or 100 μM FBP for 30 min on ice before layering on a 10–40% sucrose gradient. For conditions involving FBP, 100 μM FBP was included in the sucrose gradient, except where indicated that PKM2 was transiently exposed to FBP. Gradients were spun at 55,000 rpm for 10 h using a Beckman TLS-55 rotor, and fractions were analyzed by SDS-PAGE or Coomassie blue staining. Coomassie blue staining intensity was quantified using IR fluorescence.

Size-exclusion chromatography. Recombinant protein or ~2 mg of cellular protein was separated on a HiPrep 16/60 Sephacryl S-200 HR column (GE) in 50 mM sodium phosphate and 150 mM sodium chloride, pH 7.2. Fractions were analyzed by UV absorbance or SDS-PAGE and western blotting.

Recombinant PKM2. Full-length human PKM2 was expressed as a His-tagged fusion protein in *E. coli* strain BL21(DE3) and isolated by nickel–nitrilotriacetic acid (Ni-NTA) affinity chromatography. For structural studies, recombinant PKM2 was further purified by size-exclusion chromatography. The final protein purity was confirmed by SDS-PAGE. Further details are given in the **Supplementary Methods**.

Protein crystallization and structure determination. For cocrystallization, PKM2 was incubated overnight at 20–25 °C in the presence of 5 mM activator (TEPP-46 or DASA-58), and crystallization trays were set up using the sitting-drop vapor diffusion method with droplets of protein solution (0.5 μl) and reservoir solution (0.5 μl). The best diffracting crystals were obtained from a reservoir solution containing 25% P3350, 0.2 M NH_4OAc and 0.1 M Bis-Tris, pH 6.5. Data collection was carried out at the Advanced Photon Source beamline 23ID-B, Argonne National Laboratory, Structural Biology Center. Data were reduced with HKL-2000 (ref. 33) (DASA-58) or HKL-3000 (ref. 34) (TEPP-46). Structures were solved by direct replacement with the isomorphous Protein Data Bank[35] entry 3GQY. Activator geometry restraints were obtained at the PRODRG[36] server. Iterations of model rebuilding, refinement and geometry validation were performed with COOT[37], REFMAC[38] and MOLPROBITY[39], respectively. Further details are given in the **Supplementary Methods**.

Protein identification by LC/MS/MS. Pyruvate kinase immunoprecipitates were separated by SDS-PAGE, and the band corresponding to pyruvate kinase by molecular weight was excised, subjected to in-gel trypsin digestion and then analyzed by reversed-phase microcapillary LC/MS/MS analysis. MS/MS spectra were searched against the concatenated target and decoy (reversed) Swiss-Prot protein database using Sequest (Proteomics Browser Software, Thermo Fisher Scientific). Peptides passing a false discovery rate threshold of 1% were accepted. Additional details are given in the **Supplementary Methods**.

Metabolism measurements. Glucose-dependent lipid synthesis was performed as described previously[31]. Lactate concentrations were measured using a YSI 7100 Select Biochemistry Analyzer (YSI Incorporated). Oxygen consumption rates were measured using a polarographic oxygen electrode[40]. Where indicated, metabolites and lipid synthesis were measured using GC/MS. For determination of [U-$^{13}C_6$] glucose enrichment in lipogenic AcCoA, A549 cells were cultured for 3 d in the presence of tracer, and the relevant metabolites were extracted using methanol and chloroform. Fatty acid methyl esters were generated from the lipid biomass by dissolving dried chloroform fractions in 50 μl of Methyl-8 reagent (Pierce) and incubating at 60 °C for 1 h. The GC/MS analysis was performed using an Agilent 6890 GC equipped with a 30-m DB-35MS capillary column connected to an Agilent 5975B MS operating under electron impact ionization at 70 eV. Mass isotopomer distributions were determined by integrating palmitate ion fragments in the *m*/*z* range 270–286. Computational estimations of AcCoA enrichment and fractional new palmitate synthesis were performed as previously described[41]. For metabolite measurement by LC/MS/MS[42], cells or snap-frozen xenograft tumor tissue were extracted with a 4:1 (v/v) ratio of MeOH and H_2O equilibrated at –80 °C, and the extracts were dried under nitrogen gas. Samples were resuspended in water and analyzed using a 5500 QTRAP triple quadrupole mass spectrometer (AB SCIEX) coupled to a Prominence ultra-fast LC system (Shimadzu) by selected reaction monitoring of metabolites in both the positive and negative ion mode. Peak areas from the total ion current for the selected reaction monitoring transition of each metabolite were integrated using MultiQuant v2.0 software (AB SCIEX). Integrated total ion current areas corresponding to metabolite concentrations were imported into Metaboanalyst[43] software for further analysis. Additional details for all metabolism measurements are provided in the **Supplementary Methods**.

ADME and pharmacokinetic and acute pharmacodynamic methods. Pharmacokinetic studies were performed in fasted male BALB/c mice. After drug administration by the respective routes, plasma samples were collected at the indicated time points, and TEPP-46 concentrations were analyzed by LC/MS/MS. Pharmacokinetics parameters (C_{max}, T_{max}, $T_{1/2}$ and area under the curve) were calculated using noncompartmental model with WinNonlin Ver 5.2 statistics software (Pharsight Corporation).

Received 7 November 2011; accepted 31 July 2012; published online 26 August 2012

References

1. Tennant, D.A., Duran, R.V. & Gottlieb, E. Targeting metabolic transformation for cancer therapy. *Nat. Rev. Cancer* **10**, 267–277 (2010).
2. Vander Heiden, M.G. Targeting cancer metabolism: a therapeutic window opens. *Nat. Rev. Drug Discov.* **10**, 671–684 (2011).
3. Vander Heiden, M.G., Cantley, L.C. & Thompson, C.B. Understanding the Warburg effect: the metabolic requirements of cell proliferation. *Science* **324**, 1029–1033 (2009).
4. Cairns, R.A., Harris, I.S. & Mak, T.W. Regulation of cancer cell metabolism. *Nat. Rev. Cancer* **11**, 85–95 (2011).
5. Levine, A.J. & Puzio-Kuter, A.M. The control of the metabolic switch in cancers by oncogenes and tumor suppressor genes. *Science* **330**, 1340–1344 (2010).
6. Trachootham, D., Alexandre, J. & Huang, P. Targeting cancer cells by ROS-mediated mechanisms: a radical therapeutic approach? *Nat. Rev. Drug Discov.* **8**, 579–591 (2009).
7. Weissleder, R. Molecular imaging in cancer. *Science* **312**, 1168–1171 (2006).
8. Christofk, H.R. *et al.* The M2 splice isoform of pyruvate kinase is important for cancer metabolism and tumour growth. *Nature* **452**, 230–233 (2008).
9. Mazurek, S. Pyruvate kinase type M2: a key regulator of the metabolic budget system in tumor cells. *Int. J. Biochem. Cell Biol.* **43**, 969–980 (2011).
10. Noguchi, T., Inoue, H. & Tanaka, T. The M1- and M2-type isozymes of rat pyruvate kinase are produced from the same gene by alternative RNA splicing. *J. Biol. Chem.* **261**, 13807–13812 (1986).
11. Clower, C.V. *et al.* The alternative splicing repressors hnRNP A1/A2 and PTB influence pyruvate kinase isoform expression and cell metabolism. *Proc. Natl. Acad. Sci. USA* **107**, 1894–1899 (2010).
12. Yamada, K. & Noguchi, T. Regulation of pyruvate kinase M gene expression. *Biochem. Biophys. Res. Commun.* **256**, 257–262 (1999).
13. Ikeda, Y., Tanaka, T. & Noguchi, T. Conversion of non-allosteric pyruvate kinase isozyme into an allosteric enzyme by a single amino acid substitution. *J. Biol. Chem.* **272**, 20495–20501 (1997).
14. Ikeda, Y. & Noguchi, T. Allosteric regulation of pyruvate kinase M2 isozyme involves a cysteine residue in the intersubunit contact. *J. Biol. Chem.* **273**, 12227–12233 (1998).
15. Ashizawa, K., Willingham, M.C., Liang, C.M. & Cheng, S.Y. *In vivo* regulation of monomer-tetramer conversion of pyruvate kinase subtype M2 by glucose is mediated via fructose 1,6-bisphosphate. *J. Biol. Chem.* **266**, 16842–16846 (1991).
16. Ashizawa, K., McPhie, P., Lin, K.H. & Cheng, S.Y. An *in vitro* novel mechanism of regulating the activity of pyruvate kinase M2 by thyroid hormone and fructose 1, 6-bisphosphate. *Biochemistry* **30**, 7105–7111 (1991).
17. Christofk, H.R., Vander Heiden, M.G., Wu, N., Asara, J.M. & Cantley, L.C. Pyruvate kinase M2 is a phosphotyrosine-binding protein. *Nature* **452**, 181–186 (2008).
18. Eigenbrodt, E., Reinacher, M., Scheefers-Borchel, U., Scheefers, H. & Friis, R. Double role for pyruvate kinase type M2 in the expansion of phosphometabolite pools found in tumor cells. *Crit. Rev. Oncog.* **3**, 91–115 (1992).
19. Anastasiou, D. *et al.* Inhibition of pyruvate kinase M2 by reactive oxygen species contributes to cellular antioxidant responses. *Science* **334**, 1278–1283 (2011).
20. Vander Heiden, M.G. *et al.* Evidence for an alternative glycolytic pathway in rapidly proliferating cells. *Science* **329**, 1492–1499 (2010).
21. Locasale, J.W., Vander Heiden, M.G. & Cantley, L.C. Rewiring of glycolysis in cancer cell metabolism. *Cell Cycle* **9**, 4253 (2010).
22. Jiang, J.K. *et al.* Evaluation of thieno[3,2-b]pyrrole[3,2-d]pyridazinones as activators of the tumor cell specific M2 isoform of pyruvate kinase. *Bioorg. Med. Chem. Lett.* **20**, 3387–3393 (2010).
23. Boxer, M.B. *et al.* Evaluation of substituted *N*,*N*′-diarylsulfonamides as activators of the tumor cell specific M2 isoform of pyruvate kinase. *J. Med. Chem.* **53**, 1048–1055 (2010).
24. Ikeda, Y., Taniguchi, N. & Noguchi, T. Dominant negative role of the glutamic acid residue conserved in the pyruvate kinase M(1) isozyme in the heterotropic allosteric effect involving fructose-1,6-bisphosphate. *J. Biol. Chem.* **275**, 9150–9156 (2000).

25. Kato, H., Fukuda, T., Parkison, C., McPhie, P. & Cheng, S.Y. Cytosolic thyroid hormone-binding protein is a monomer of pyruvate kinase. *Proc. Natl. Acad. Sci. USA* **86**, 7861–7865 (1989).
26. Hitosugi, T. *et al.* Tyrosine phosphorylation inhibits PKM2 to promote the Warburg effect and tumor growth. *Sci. Signal.* **2**, ra73 (2009).
27. Lv, L. *et al.* Acetylation targets the M2 isoform of pyruvate kinase for degradation through chaperone-mediated autophagy and promotes tumor growth. *Mol. Cell* **42**, 719–730 (2011).
28. Luo, W. *et al.* Pyruvate kinase M2 is a PHD3-stimulated coactivator for hypoxia-inducible factor 1. *Cell* **145**, 732–744 (2011).
29. Hoshino, A., Hirst, J.A. & Fujii, H. Regulation of cell proliferation by interleukin-3–induced nuclear translocation of pyruvate kinase. *J. Biol. Chem.* **282**, 17706–17711 (2007).
30. Steták, A. *et al.* Nuclear translocation of the tumor marker pyruvate kinase M2 induces programmed cell death. *Cancer Res.* **67**, 1602–1608 (2007).
31. Hatzivassiliou, G. *et al.* ATP citrate lyase inhibition can suppress tumor cell growth. *Cancer Cell* **8**, 311–321 (2005).
32. Vander Heiden, M.G. *et al.* Identification of small molecule inhibitors of pyruvate kinase M2. *Biochem. Pharmacol.* **79**, 1118–1124 (2010).
33. Otwinowski, Z. & Minor, W. Processing of X-ray diffraction data collected in oscillation mode. in *Methods in Enzymology* Vol. 276, 307–326 (Academic Press, 1997).
34. Minor, W., Cymborowski, M., Otwinowski, Z. & Chruszcz, M. HKL-3000: the integration of data reduction and structure solution—from diffraction images to an initial model in minutes. *Acta Crystallogr. D Biol. Crystallogr.* **62**, 859–866 (2006).
35. Berman, H.M. *et al.* The Protein Data Bank. *Nucleic Acids Res.* **28**, 235–242 (2000).
36. Schüttelkopf, A.W. & van Aalten, D.M. PRODRG: a tool for high-throughput crystallography of protein-ligand complexes. *Acta Crystallogr. D Biol. Crystallogr.* **60**, 1355–1363 (2004).
37. Emsley, P., Lohkamp, B., Scott, W.G. & Cowtan, K. Features and development of Coot. *Acta Crystallogr. D Biol. Crystallogr.* **66**, 486–501 (2010).
38. Murshudov, G.N., Vagin, A.A. & Dodson, E.J. Refinement of macromolecular structures by the maximum-likelihood method. *Acta Crystallogr. D Biol. Crystallogr.* **53**, 240–255 (1997).
39. Davis, I.W., Murray, L.W., Richardson, J.S. & Richardson, D.C. MOLPROBITY: structure validation and all-atom contact analysis for nucleic acids and their complexes. *Nucleic Acids Res.* **32**, W615–W619 (2004).
40. Schumacker, P.T., Chandel, N. & Agusti, A.G. Oxygen conformance of cellular respiration in hepatocytes. *Am. J. Physiol.* **265**, L395–L402 (1993).
41. Metallo, C.M. *et al.* Reductive glutamine metabolism by IDH1 mediates lipogenesis under hypoxia. *Nature* **481**, 380–384 (2011).
42. Yuan, M., Breitkopf, S.B., Yang, X. & Asara, J.M. A positive/negative ion-switching, targeted mass spectrometry-based metabolomics platform for bodily fluids, cells, and fresh and fixed tissue. *Nat. Protoc.* **7**, 872–881 (2012).
43. Xia, J., Mandal, R., Sinelnikov, I.V., Broadhurst, D. & Wishart, D.S. MetaboAnalyst 2.0–a comprehensive server for metabolomic data analysis. *Nucleic Acids Res.* W127–W133 (2012).

Acknowledgments

The Structural Genomics Consortium is a registered charity (1097737) and receives funds from the Canadian Institutes for Health Research, the Canadian Foundation for Innovation, Genome Canada through the Ontario Genomics Institute, GlaxoSmithKline, Karolinska Institutet, the Knut and Alice Wallenberg Foundation, the Ontario Innovation Trust, the Ontario Ministry for Research and Innovation, Merck and Co., Inc., the Novartis Research Foundation, the Swedish Agency for Innovation Systems, the Swedish Foundation for Strategic Research and the Wellcome Trust. The crystallography results shown in this report are derived from work performed at Argonne National Laboratory, Structural Biology Center at the Advanced Photon Source. Argonne is operated by UChicago Argonne, LLC for the US Department of Energy, Office of Biological and Environmental Research under contract DE-AC02-06CH11357. We thank P. Chang for experimental advice related to sucrose gradient ultracentrifugation and SAI Advantium Pharma Ltd. for help with pharmacokinetics studies. We also thank M. Kini for experimental help and acknowledge M. Yuan and S. Breitkopf for help with MS experiments. This work was supported by the Molecular Libraries Initiative of the NIH Roadmap for Medical Research and the Intramural Research Program of the National Human Genome Research Institute, NIH and by NIH grant R03MH085679. This work was also funded by NIH grant R01 GM56203 (L.C.C.). J.M.A. acknowledges funding from NIH 5P01CA120964 and Dana-Farber/Harvard Cancer Center support grant NIH 5P30CA006516. M.G.V.H. acknowledges additional funding support from the Smith Family Foundation, the Burroughs Wellcome Fund, the Damon Runyon Cancer Research Foundation, the Stern family and the National Cancer Institute, including NIH 5P30CA1405141.

Author contributions

D.A., Y.Y., W.J.I. and M.G.V.H. designed and coordinated the study. M.B.B., C.J.T., L.C.C., H.-W.P. and L.D. advised on various aspects of the study. J.-K.J., M.B.B., M.S., A.P.S., H.V., N.S., M.J.W., K.R.B., W.L., C.P.A., J.I., D.S.A. and C.J.T. designed and provided compounds. B.S.H., W.T., S.D. and H.-W.P. performed all structural studies. A.J. did additional structural analysis. H.Y., C.K., K.E.Y., K.K., F.G.S., S.J. and L.D. performed *in vivo* pharmacology and ADME studies. C.M.M., J.M.A. and G.S. did MS. M.H.H. reviewed pathology. D.A., Y.Y., W.J.I., K.R.M., B.P.F., K.D.C., S.M., T.M.K., C.K., S.Y.L., Z.R.J., S.M.D., H.R.C. and M.G.V.H. all performed experiments. D.A. and M.G.V.H. wrote the paper with substantial input from Y.Y. and W.J.I.

Competing financial interests

The authors declare competing financial interests: details accompany the online version of the paper.

Additional information

Supplementary information and chemical probe information is available in the online version of the paper. Reprints and permissions information is available online at http://www.nature.com/reprints/index.html. Correspondence and requests for materials should be addressed to M.G.V.H.